RSC Advances

PAPER

View Article Online
View Journal | View Issue

Cite this: *RSC Adv.*, 2026, **16**, 17305

Fluorescence-enhanced BINOL-hybridized ladder-type siloxanes and their sensing of Fe^{3+}

Keqian Zou,[a] Rongrong He,[a] Lizhong Zeng,[a] Yujia Liu,[b] Zheng Xu,[a] Masafumi Unno,*[b] Liwen Xu*[a] and Zhanjiang Zheng*[a]

Received 2nd February 2026
Accepted 25th March 2026

DOI: 10.1039/d6ra00896h

rsc.li/rsc-advances

In this study, we synthesized two novel vinyl-substituted, BINOL-hybridized tricyclic-ladder-type siloxanes (referred to as Vi-TLS-BINOLs) *via* a $B(C_6F_5)_3$-catalyzed Piers–Rubinsztajn reaction. Fluorescence studies of the Vi-TLS-BINOLs revealed enhanced fluorescence emission attributed to the restricted intramolecular motion by the ladder-type structure. In comparison to the precursor BINOL, Vi-TLS-BINOLs **L1** and **L2** exhibit a 5.2-fold and 4.8-fold increase in fluorescence quantum yield in THF, respectively. Furthermore, it was observed that both Vi-TLS-BINOLs could selectively recognize Fe^{3+} through fluorescence quenching. ESI-HRMS analysis confirmed the formation of [**L1** + 2Fe] and [**L1** + 3Fe] complexes with Fe^{3+}. The detection limits for Fe^{3+} were determined to be 10.6 μM and 16.3 μM, respectively.

Introduction

Silsesquioxanes (SQs) with $RSiO_{1.5}$ repeat units have gained significant attention due to their hybridized nature, which combines organic and inorganic siloxane components, resulting in good processability, high thermal stability and excellent biocompatibility. These properties have enabled the use of SQs in a variety of fields, such as biomaterials, dielectric materials, and organic light-emitting diode (OLEDs) devices.[1–4] Three primary categories of SQs have been recognized: fully condensed silsesquioxanes, incompletely condensed silsesquioxanes (*e.g.*, DDSQ-type), and ladder-type silsesquioxanes.[5–8] The latter, referred to as "ladder-type", describes SQs that possess more than two fused siloxane rings arranged in a stereoregular double-chain structure. Of particular interest are hybridized ladder-type modified SQs, which consist of an inorganic siloxane core connected to two hybridized macrocyclic side-rings containing both siloxane and organic moieties.[9] In this context, triazole-hybridized ladder-type siloxanes were recently developed by our group for the selective detection of iodide ions through cooperative hydrogen-bonding.[10] Furthermore, phenyl-substituted BINOL-hybridized ladder-type siloxanes (TLS-BINOLs) have been synthesized, exhibiting exceptional specificity in the sensing of fluoride ions through a structural breakdown mechanism initiated by fluoride.[11] Despite the research on these materials, there have been no reports of hybridized ladder-type siloxanes being used for sensing metal cations.

Iron is a vital metal found on Earth that is essential for the majority of life forms and human health. It is a key component of proteins and enzymes vital for sustaining good health, playing an important role in oxygen metabolism, oxygen transportation, and electron transfer.[12–14] An imbalance in Fe^{3+} levels can significantly impart metabolism and cell homeostasis, leading to a variety of diseases including anemia, chronic renal disease, and hemochromatosis.[12–14] To address this issue, various techniques have been developed for the detection of iron ions, with fluorescence spectroscopy being particularly effective for its high sensitivity, selectivity, and cost-effectiveness.[15–18] However, the preparation of these sensors is laborious and requires complex procedures.[19–24] Therefore, the design and synthesis of novel and easily-accessible sensors remains a challenge.

1,1′-Binaphthalene-2,2′-diol (BINOL) and its derivatives, which are characterized by biaryl compounds exhibiting axial chirality and two active phenolic hydroxyl groups, as well as being easily modifiable, have attracted significant attention in fluorescence-based molecular recognition.[25–30] In connecting with our continuing research on chemosensors utilizing the BINOL fluorophore,[10,11,31–33] we report herein two novel vinyl-substituted, tricyclic-ladder-type siloxanes hybridized with BINOL (Vi-TLS-BINOLs), prepared *via* the Piers–Rubinsztajn reaction (Scheme 1). Their distinctive structure comprises a central siloxane ring and two side rings, each containing five oxygens. This unique structure suggests the potential for accommodating metal ions through a "host–guest" recognition process within their macrocyclic cavities. Further Fluorescence spectroscopy study showed that Vi-TLS-BINOLs possess the

[a]*College of Material, Chemistry and Chemical Engineering, Key Laboratory of Organosilicon Chemistry and Material Technology, Ministry of Education, Zhejiang Key Laboratory of Organosilicon Material Technology, Hangzhou Normal University, Hangzhou, 311121, China. E-mail: liwenxu@hznu.edu.cn; zzjiang78@hznu.edu.cn*

[b]*Department of Chemistry and Chemical Biology, Graduate School of Science and Technology, Gunma University, Kiryu 376-8515, Japan. E-mail: unno@gunma-u.ac.jp*

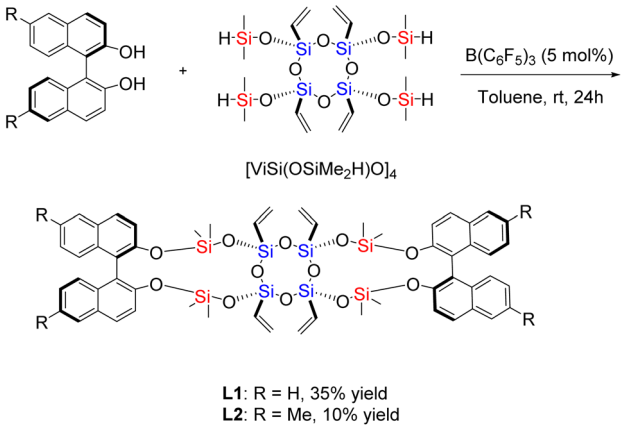

Scheme 1 Synthesis of the new vinyl substituted BINOL-hybrided tricyclic ladder-type siloxanes **L1** and **L2**.

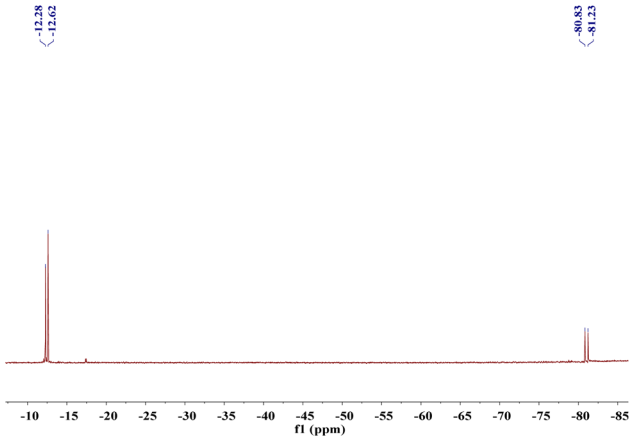

Fig. 1 ^{29}Si NMR spectra (in acetone-d_6) for the compound **L1**.

capability to selectively recognize iron ions through a quenching process.

Results and discussion

One of the chosen starting materials for this investigation is hydrosilyl-substituted all-*cis*-tetravinylcyclotetrasiloxane $[ViSi(OSiMe_2H)O]_4$,[34] which can be readily prepared from the reaction of all-*cis*-tetravinylcyclotetrasilanolate $[ViSi(OK)O]_4$ and chlorodimethylsilane. The other starting material is *R*-BINOL or 6-methyl-*R*-BINOL. As shown in Scheme 1, these two precursors undergo cyclization *via* the Piers–Rubinsztajn reaction,[35–37] wherein the Si–H groups of $[ViSi(OSiMe_2H)O]_4$ react with the –OH groups of BINOL catalyzed by the Lewis acid $B(C_6F_5)_3$, producing the desired ladder-type siloxanes with well-defined structures.

The hybridized ladder-type siloxanes **L1** and **L2** were fully characterized using ^{1}H, ^{13}C, ^{29}Si NMR, and HRMS-ESI. The ^{1}HNMR data of **L1** (see Fig. S13) confirmed the complete functionalization of Si–H groups, as evidenced by the absence of resonances for Si–H groups (4.74 ppm) from the precursor $[ViSi(OSiMe_2H)O]_4$. Signals ranging from 5.09 to 6.14 ppm corresponding to the vinyl groups, and four singlet signals (−0.22, −0.18, 0.23, 0.31 ppm) of the methyl protons of Si–$(CH_3)_2$ were observed, attributed to the axial chirality of the BINOL and the constrained rotation of (Me_2)Si–O bonds from the cyclic structure of **L1**. The ^{13}C NMR spectrum of **L1** (see Fig. S14) displayed four characteristic signals at −0.06, 0.01, 0.30, and 0.77 ppm corresponding to the carbon of Si–$(CH_3)_2$. The ^{29}Si NMR (see Fig. 1) analysis of **L1** showed two sets of signals, attributed to the T-unit silicon atoms (Si in blue, −80.83 and −81.23 ppm) and D-unit silicon atoms (Si in red, −12.28 and −12.62 ppm), respectively. HRMS-ESI mass spectroscopy was utilized to characterize compound **L1** further. The results aligned with the calculated mass of ($[M + Na]^+$ calcd for $C_{56}H_{60}NaO_{12}Si_8$: 1171.2137; found: 1171.2125). Additionally, the isotopic distribution pattern on the mass spectrum matched the calculated pattern well (refer to Fig. S9).

The UV absorption bands observed in the ladder hybridized molecule are ascribed to the transitions of the binaphthyl rings (See Fig. 2a), specifically the ^1B_b transition occurring between 230 and 250 nm, the ^1L_a transition spanning from 250 to 300 nm, and the ^1L_b transition ranging from 300 to 350 nm. As shown in Fig. 2b, the fluorescence spectra (λ_{ex} = 260 nm) of **L1** and **L2** in THF solution displayed emission bands at 355 and 359 nm respectively. Their quantum yields (Φ_F, see Table 1) in THF (1.0×10^{-5} M) were found to be 11.9% and 11.1% respectively. These values are significantly higher than the quantum yield of the precursor BINOL (2.3%). Furthermore, in their powder forms, **L1** and **L2** exhibited drastically increased fluorescence (Φ_F = 41.3% and 20.4% respectively), which remain higher than that of the solid precursor BINOL (13.7%). The enhanced fluorescence of **L1** and **L2** is proposed to result from the restriction of intramolecular motion induced by the ladder-type structure. This structure effectively immobilizes the BINOL chromophores within the ladder skeleton, thereby inhibiting non-radiative processes.[38,39] Consequently, this phenomenon is referred to as ladderization-induced emission enhancement (LIEE), which is conceptually grounded in the well-established principle of restriction of intramolecular motion (RIM).[40] In many flexible fluorophores, excited-state energy is readily dissipated through non-radiative channels such as torsional rotations and other vibrational modes.[41] By covalently locking the BINOL units into a rigid ladder architecture at the single-molecule level, these non-radiative decay pathways are effectively minimized. This strategy is distinct

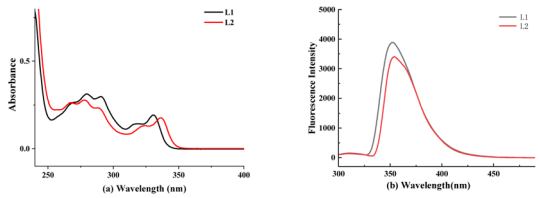

Fig. 2 (a) UV absorption spectra of compound **L1**-**L2** in 10 μM THF; (b) fluorescence emission spectra (λ_{ex} = 260 nm) of compound **L1**-**L2** in 10 μM THF.

Table 1 Quantum yields of *R*-BINOL and corresponding ladder-type siloxanes **L1** and **L2**

	R-BINOL	Ladder **L1**	Ladder **L2**
Φ_F (%) (solid)	13.7	41.3	20.4
Φ_F (%) (in THF)	2.3	11.9	11.1

from, yet complementary to, the widely studied phenomenon of aggregation-induced emission (AIE). In AIE systems, emission is activated by the formation of intermolecular aggregates in poor solvents or the solid state, which physically hinders intramolecular rotations. In contrast, LIEE achieves this restriction at the single-molecule level through robust covalent bonds. Consequently, **L1** and **L2** are already significantly more emissive than their precursor in dilute solution.

The recognition ability of compound **L1** towards perchlorate salts of various metals (Fe^{3+}, Ag^+, Al^{3+}, Ca^{2+}, Cd^{2+}, Cu^{2+}, K^+, Li^+, Mn^{2+}, Na^+, NH_4^+, Pb^{2+}, Zn^{2+}) was investigated using fluorescence spectroscopy in THF solutions ($\lambda_{ex} = 260$ nm, see Fig. 3). Addition of 50 equivalents of each metal revealed that Fe^{3+} significantly reduced fluorescence intensity at 355 nm, Cu^{2+} caused half quenching, while other metal ions had slight impact on fluorescence emission. Further experiments showed that 50 equivalents of Fe^{3+} led to up to 99% quenching in MeOH, compared to 93% quenching in THF. Subsequent fluorescence titration experiments in MeOH demonstrated a incremental reduction in fluorescence intensity at 355 nm with increasing Fe^{3+} concentrations, as shown in Fig. 4. The quenching response was analyzed using a Stern–Volmer plot (see Fig. S3), with the equation $F_0/F = K_{sv}[Q] + 1$, where F_0 and F represent fluorescence intensity in the absence and presence of Fe^{3+}, respectively, and $[Q]$ is the molar concentration of quencher Fe^{3+}. This analysis yielded a calculated quenching constant (K_{sv}) of 2.2×10^4. The K_{sv} value for compound **L2** was determined to be 2.8×10^4 similarly. The high K_{sv} values, along with the nonlinear behavior observed, suggest the formation of

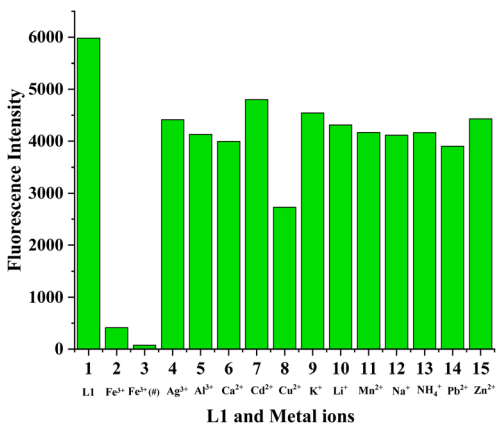

Fig. 3 Fluorescence emission data ($\lambda_{ex} = 260$ nm) of compound **L1** with the addition of various metal ions (50 equivalents) in 10 μM THF, and iron ions (50 equivalents, Fe^{3+}(#)) in 10 μM MeOH.

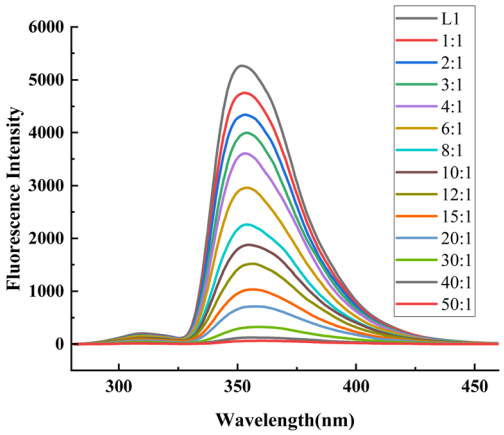

Fig. 4 Fluorescence emission spectra ($\lambda_{ex} = 260$ nm) of compound **L1** (10 μM) in MeOH with the increasing concentration of Fe^{3+}, inset displays a Stern–Volmer plot of **L1** upon addition of Fe^{3+} in MeOH.

a non-fluorescent complex in the ground state, likely due to the oxygen atoms' capability to coordinate with iron ions, resulting in fluorescence quenching.[42,43] Furthermore, the fluorescence response of **L1** to Fe^{3+} was assessed in solutions buffered at pH 4, 7, and 10 to determine the impact of pH on sensing performance (see Fig. S11). Addition of 15 equivalents of Fe^{3+} resulted in largely consistent fluorescence intensities across the pH range tested. Complete fluorescence quenching occurred with 40 equivalents of Fe^{3+}, regardless of the pH of the solution. Sensor **L2** exhibited a similar response pattern (Fig. S12), suggesting limited influence of pH on the sensing capabilities of these two sensors.

In the investigation of the Fe^{3+} calibration curve for compound **L1**, a linear relationship was examined within the concentration range of 0–200 μM in Fig. S5. Through meticulous data processing and statistical analysis, a highly linear calibration curve was established with a correlation coefficient (R^2) of 0.96, indicating a robust degree of data fitting. The detection limit was determined utilizing the standard $3\sigma/K$ method, involving the calculation of the standard deviation σ from 10 blank tests and the utilization of the calibration curve's gradient K, resulting in a Fe^{3+} detection limit of 10.6 μM. For compound **L2**, the same approach was employed, yielding a Fe^{3+} detection limit of 16.3 μM as inferred from the data analysis presented in Fig. S6. Both compounds demonstrated comparable detection performance (Table S1), affirming the reliability and precision of the developed methodology.

Competitive metal binding experiments in MeOH were conducted to assess the selectivity of compound **L1** for Fe^{3+} ions amidst a complex mixture of potentially interfering species, including Ag^+, Al^{3+}, Ca^{2+}, Cd^{2+}, Cu^{2+}, K^+, Li^+, Mn^{2+}, Na^+, NH_4^+, Pb^{2+}, Zn^{2+} (30 equiv.) (Fig. 5). Analysis of the fluorescence intensity depicted in Fig. 5 revealed no significant changes when comparing the profiles with and without the presence of other metal ions. Notably, only K^+ exhibited a minor impact on the quenching process, indicating the high selectivity of compound **L1** for Fe^{3+} ions. Furthermore, parallel competitive binding experiments conducted with **L2** across diverse

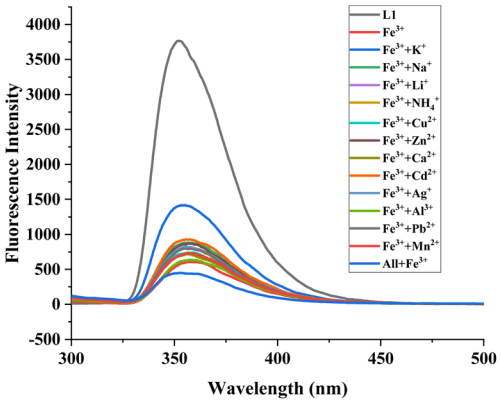

Fig. 5 Fluorescent emission responses of **L1** (2.5 μM) with different perchlorate salts of metal ions (30 equiv.) in the presence or absence of Fe^{3+} (30 equiv.) in MeOH.

interfering metals demonstrated a similarly reliable sensing capability (Fig. S7), thereby confirming the robustness of this sensor design.

The structure of the BINOL-hybridized compound **L1** was optimized to investigate its properties. The HOMO/LUMO molecular orbitals were calculated using the Gaussian 03 program at the B3LYP/6-31G(d,p) level (refer to Fig. 6). The electron densities of the HOMO in compound **L1** were observed to be distributed along the binaphthyl rings and oxygen atoms, creating an electron cloud cavity capable of encapsulating iron ions during the recognition process. To further elucidate the interaction between **L1** and iron ions, ESI-MS analysis was performed on a mixture of Fe^{3+} and ladder-type siloxane **L1** in methanol (refer to Fig. S8). The ion peaks detected at *m*/*z* 1261.0900 and 1317.0468 correspond to [**L1** + 2Fe] and [**L1** + 3Fe] complexes, indicating the formation of complexes between Fe^{3+} and ladder-type siloxane **L1** at molar ratios of 2 : 1 and 3 : 1, respectively. These results suggest that ladder-type siloxane **L1** chelates with iron ions through the oxygens of BINOL and T4-siloxane, leading to the formation of cavity-captured complexes with stoichiometries of 2 : 1 or 3 : 1. This nonfluorescent complex is believed to be responsible for the observed decrease in fluorescence intensity, where the electrons in the excited state will transfer to the half-filled 3d orbitals of the paramagnetic Fe^{3+}, leading to the fluorescence quenching of ladder-Fe^{3+} complex with the nonradiative electronehole annihilation.[44]

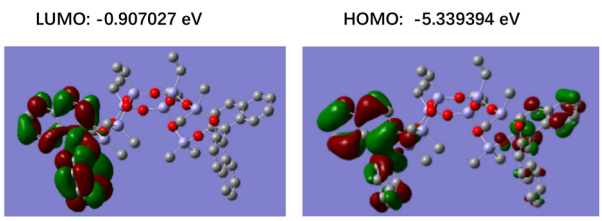

Fig. 6 The shape and energy of the HOMO and LUMO orbitals of compound **L1** calculated at the DFT level using a B3LYP/6-31G(d,p) basis set.

Conclusions

In summary, two novel vinyl-substituted, BINOL hybridized tricyclic ladder-type siloxane compounds (Vi-TLS-BINOLs) have been successfully synthesized *via* the $B(C_6F_5)_3$-catalyzed Piers–Rubinsztajn reaction of the BINOL precursor and hydrosilyl-substituted all-*cis*-tetravinylcyclotetrasiloxane. These Vi-TLS-BINOLs demonstrated Ladderization-Induced Emission Enhancement (LIEE) attributed to the restricted intramolecular motion resulting from the hybridization of BINOL with all-*cis*-tetravinylcyclotetrasiloxane. Furthermore, fluorescence studies have showed that Vi-TLS-BINOLs can selectively recognize Fe^{3+} in the presence of various competitive ions, leading to effective fluorescence quenching caused by the formation of the nonfluorescent [**L1** + 2Fe] and [**L1** + 3Fe] complexes.

Author contributions

Conceptualization: Z. Z., L. X. and M. U.; methodology: Z. Z., K. Z., R. H. and L. Z.; formal analysis and investigation: K. Z., R. H., Y. L. and Z. X.; writing – original draft preparation: Z. Z. and K. Z.; writing – review and editing: Z. Z., M. U. and L. X.; funding acquisition: Z. Z, L. X. and M. U.

Conflicts of interest

There are no conflicts to declare.

Data availability

All relevant data required to reproduce the findings of this study are incorporated into the article or available in the online supplementary information (SI). Supplementary information: NMR spectra of **L1** and **L2**, fluorescence titration spectra, HRMS-ESI spectra, and list of the reported molecules for sensing Fe^{3+}. See DOI: https://doi.org/10.1039/d6ra00896h.

Acknowledgements

The authors acknowledge the financial support from the National Natural Science Foundation of China (No. 22072035) and the New Energy and Industrial Technology Development Organization (NEDO, No. JPNP06046).

Notes and references

1 R. H. Baney, M. Itoh, A. Sakakibara and T. Suzuki, *Chem. Rev.*, 1995, **95**, 1409.
2 D. B. Cordes, P. D. Lickiss and F. Rataboul, *Chem. Rev.*, 2010, **110**, 2081.
3 B. A. Kamino and T. P. Bender, *Chem. Soc. Rev.*, 2013, **42**, 5119.
4 V. Ervithayasuporn, J. Abe, X. Wang, T. Matsushima, H. Murata and Y. Kawakami, *Tetrahedron*, 2010, **66**, 9348.
5 R. M. Laine and M. F. Roll, *Macromolecules*, 2011, **44**, 1073.
6 B. Dudziec and B. Marciniec, *Curr. Org. Chem.*, 2018, **21**, 2794.

7 Y. Du and H. Liu, *Dalton Trans.*, 2020, **49**, 5396.
8 M. Unno, A. Suto and T. Matsumoto, *Russ. Chem. Rev.*, 2013, **82**, 289.
9 Z. J. Zheng, Y. J. Liu, N. Takeda and M. Unno, *Dalton Trans.*, 2023, **52**, 9737.
10 Z. Zheng, N. Yagafarov, Z. Xu, A. Ouali, N. Takeda, Y. Liu and M. Unno, *Dalton Trans.*, 2023, **52**, 10298.
11 R. He, Y. Liu, X. Yang, Z. Zheng, Z. Xu, N. Takeda, M. Unno and L. Xu, *Inorg. Chem.*, 2023, **62**, 14991.
12 S. K. Sahoo, D. Sharma, R. K. Bera, G. Crisponi and J. F. Callan, *Chem. Soc. Rev.*, 2012, **41**, 7195.
13 H. Chen, P. Fan, X. Tu, H. Min, X. Yu, X. Li, J. L. Zeng, S. Zhang and P. Cheng, *Chem.–Asian J.*, 2019, **14**, 3611.
14 M. Kumar, R. Kumar and V. Bhalla, *Org. Lett.*, 2010, **13**, 366.
15 W. P. Lustig, S. Mukherjee, N. D. Rudd, A. V. Desai, J. Li and S. K. Ghosh, *Chem. Soc. Rev.*, 2017, **46**, 3242.
16 L. E. Kreno, K. Leong, O. K. Farha, M. Allendorf, R. P. Van Duyne and J. T. Hupp, *Chem. Rev.*, 2011, **112**, 1105.
17 H. Chen, L. Li, Z. Zhu, J. Li, J. Tu, H. Liu, *et al.*, *Chin. Chem. Lett.*, 2026, DOI: 10.1016/j.cclet.2026.112400.
18 J. Li, Y. Hou, H. Wu, C. Chen, X. Fu, J. Liu, *et al.*, *Colloids Surf., B*, 2025, **247**, 114421.
19 V. Bhalla, A. Gupta and M. Kumar, *Talanta*, 2013, **105**, 152.
20 N. Omer, F. Zhang, G. Zhao, S. Guang and H. Xu, *Analyst*, 2019, **144**, 3414.
21 S. Chatterjee, X. S. Li, F. Liang and Y. W. Yang, *Small*, 2019, **15**, 1904569.
22 Y. Ma, W. Luo, P. J. Quinn, Z. Liu and R. C. Hider, *J. Med. Chem.*, 2004, **47**, 6349.
23 S. Munusamy and S. Kulathu Iyer, *Tetrahedron: Asymmetry*, 2016, **27**, 492.
24 K. D. Bhatt, H. S. Gupte, B. A. Makwana, D. J. Vyas, D. Maity and V. K. Jain, *J. Fluoresc.*, 2012, **22**, 1493.
25 L. Pu, *Acc. Chem. Res.*, 2012, **45**, 150.
26 J. Wen, L. Dong, J. Tian, T. Jiang, Y. Yang, Z. Huang, X. Yu, C. Hu, S. Hu, T. Yang and X. Wang, *J. Hazard. Mater.*, 2013, **263**, 638.
27 L. Pu, *Acc. Chem. Res.*, 2017, **50**, 1032.
28 Y. Y. Zhu, X. D. Wu, S. X. Gu and L. Pu, *J. Am. Chem. Soc.*, 2019, **141**, 175.
29 S. Yu, A. M. DeBerardinis, M. Turlington and L. Pu, *J. Org. Chem.*, 2011, **76**, 2814.
30 M. Q. Wang, K. Li, J. T. Hou, M. Y. Wu, Z. Huang and X. Q. Yu, *J. Org. Chem.*, 2012, **77**, 8350.
31 F. Li, L. Li, W. Yang, L. S. Zheng, Z. J. Zheng, K. Z. Jiang, Y. X. Lu and L. W. Xu, *Tetrahedron Lett.*, 2013, **54**, 1584.
32 C. Y. Wang, J. F. Zou, Z. J. Zheng, W. S. Huang, L. Li and L. W. Xu, *RSC Adv.*, 2014, **4**, 54256.
33 F. Li, Z. J. Zheng, J. Y. Shang, K. Z. Jiang, G. Q. Lai, J. X. Jiang and L. W. Xu, *Chem.–Asian J.*, 2012, **7**, 2008.
34 T. Chaiprasert, Y. J. Liu, P. K. Intaraprecha, R. Kunthom, N. Takeda and M. Unno, *Macromol. Rapid Commun.*, 2021, **42**, 2000608.
35 S. E. Laengert, A. F. Schneider, E. Lovinger, Y. Chen and M. A. Brook, *Chem.–Asian J.*, 2017, **12**, 1208.
36 L. Ai, Y. Chen, L. He, Y. Luo, S. Li and C. Xu, *Chem. Commun.*, 2019, **55**, 14019.
37 M. Melendez-Zamudio, K. Chavda and M. A. Brook, *Molecules*, 2022, **27**, 1869.
38 S. Li, K. Liu, X.-C. Feng, Z.-X. Li, Z.-Y. Zhang, B. Wang, M. Li, Y.-L. Bai, L. Cui and C. Li, *Nat. Commun.*, 2022, **13**, 2850.
39 N. L. C. Leung, N. Xie, W. Yuan, Y. Liu, Q. Wu, Q. Peng, Q. Miao, J. W. Y. Lam and B. Z. Tang, *Chem.–Eur. J.*, 2014, **20**, 15349.
40 Y. Tu, Z. Zhao, J. W. Y. Lam and B. Z. Tang, *Natl. Sci. Rev.*, 2021, **8**, nwaa260.
41 F. Bu, R. Duan, Y. Xie, Y. Yi, Q. Peng, R. Hu, *et al.*, *Angew. Chem., Int. Ed.*, 2015, **54**, 14492.
42 J. L. Bricks, A. Kovalchuk, C. Trieflinger, M. Nofz, M. Büschel, A. I. Tolmachev, J. Daub and K. Rurack, *J. Am. Chem. Soc.*, 2005, **127**, 13522.
43 R. Nudelman, O. Ardon, Y. Hadar, Y. Chen, J. Libman and A. Shanzer, *J. Med. Chem.*, 1998, **41**, 1671.
44 Y. Song, C. Z. Zhu, J. H. Song, H. Li, D. Du and Y. H. Lin, *ACS Appl. Mater. Interfaces*, 2017, **9**, 7399.